Cell Communication and Signaling

RESEARCH

Open Access

IKZF1 as a potential therapeutic target for dendritic cell-mediated immunotherapy in IgA nephropathy

Fei Peng[1,2†], Chunjia Sheng[2†], Jiayi He[3†], Yena Zhou[1,2], Yilun Qu[2], Shuwei Duan[2], Yinghua Zhao[4], Jikai Xia[2], Jie Wu[2], Guangyan Cai[2], Lingling Wu[2*], Chuyue Zhang[2,5*] and Xiangmei Chen[1,2,5*]

Abstract

Background Immunoglobulin A nephropathy (IgAN) is the most common primary glomerulonephritis globally and a major cause of renal failure. Immune dysregulation drives its pathogenesis. This study identifies novel genes as potential diagnostic and therapeutic targets, elucidating immune mechanisms in IgAN.

Methods Immune cell infiltration analysis was conducted to explore the abnormal regulation of immune cells in IgAN. Weighted gene co-expression network analysis (WGCNA) was integrated with protein-protein interaction (PPI) analysis to identify hub genes associated with dendritic cells (DCs) in IgAN. Receiver operating characteristic (ROC) curve analysis and machine learning algorithms were employed to screen for DC-related diagnostic biomarkers from the dataset. Multiple bioinformatics methods were utilized to reveal shared molecular pathways. The findings were further validated through in vivo and vitro intervention experiments.

Results WGCNA, Cytoscape, and three machine learning models collectively identified hub genes (IKZF1, MPEG1, CCR2, CCR5, and CCR7) that are significantly associated with DC immunity. Among these, IKZF1 was pinpointed as a key hub gene and a potential diagnostic biomarker for DC-related immune responses. Gene Ontology (GO), Kyoto Encyclopedia of Genes and Genomes (KEGG) pathway analysis, and gene set enrichment analysis (GSEA) further revealed substantial differences in the biological processes, signaling pathways, and immune characteristics of DCs. RT-qPCR and immunofluorescence analyses confirmed enhanced infiltration of $IKZF1^{+}$ DCs in the tissues of both IgAN mice and anti-Thy1 nephritis rats. Mechanistically, IKZF1 promotes inflammation by mediating the production of pro-inflammatory factors and enhancing antigen presentation in DCs; this effect can be mitigated by siIKZF1 or lenalidomide treatment under LPS-induced inflammatory conditions in vitro. Consistently, treatment with

†Fei Peng, Chunjia Sheng and Jiayi He contributed equally to this work

*Correspondence:
Lingling Wu
wulingling19860328@163.com
Chuyue Zhang
zhangcycywch@wchscu.edu.cn
Xiangmei Chen
xmchen301@126.com

Full list of author information is available at the end of the article

lenalidomide, a molecular degrader of IKZF1, in anti-Thy1 nephritis models effectively alleviated renal damage and reduced inflammatory cell infiltration.

Conclusions This study delineated key patterns of immune cell infiltration in IgAN and identified diagnostic biomarkers associated with DCs, offering valuable insights into the potential therapeutic targeting of IKZF1$^+$ DCs.

Keywords Computational biology, Dendritic cells, Immunoglobulin A nephropathy, IKZF1, Biomarkers

Background

Immunoglobulin A nephropathy (IgAN) is the most common primary glomerulonephritis worldwide and is the leading cause of kidney failure. Up to 20-40% of adult patients with IgAN develop end stage renal disease within 10 to 20 years after diagnosis [1, 2]. Severe glomerulosclerosis and chronic tubulointerstitial changes are believed to be the strongest histopathological risk factors for a poor prognosis in patients with IgAN [3].

Recent reports have identified IgAN as an autoimmune disease and a multi-hit hypothesis has been proposed to elucidate its pathogenesis [4]. The pathogenesis and progression of IgAN are significantly influenced by both innate and adaptive immunity [5]. The deposition of immune complexes triggers the production of inflammatory mediators by glomerular mesangial cells and podocytes, establishing an inflammatory microenvironment [6]. Subsequently, immune cells (such as macrophages, dendritic cells (DCs), and T cells aggregate in local glomeruli and glomeruli of the proximal nephrons, driving disease progression [7]. Importantly, immune cell infiltration in the renal tubulointerstitium has been identified as a significant factor contributing to poor clinical outcomes in adult IgAN patients [8, 9]. CD68$^+$ macrophage aggregation and CD3$^+$ or CD8$^+$ lymphocyte infiltration are considered predictive markers for the progression of IgAN [7]. Tissue-infiltrating B cells secrete proinflammatory cytokines, chemokines, and immunoglobulins, which recruit additional lymphocytes and activate resident renal cells, exacerbating renal inflammation and contributing to renal fibrosis and functional decline [10]. The prevailing belief is that IgAN is an immune-related disease, and that DCs collectively contribute to the pathogenesis of the disease and play a pivotal role in its progression.

DCs can express various co-stimulatory molecules, cytokines, and chemokines that exert their effects on both innate immune cells and renal parenchymal cells, thereby inducing adaptive immunity through antigen presentation to T cells [11, 12]. Multiple studies have consistently demonstrated the pathogenic role of DCs in various kidney diseases, such as experimental nephrotoxic nephritis, glomerulonephritis, and lupus nephritis, thereby underscoring the critical involvement of DCs in the initiation and progression of renal diseases.

This study identifies DC-related hub genes in the setting of IgAN using weighted gene co-expression network analysis (WGCNA) and machine learning. A previously uploaded dataset, GSE175759 [13] from the Gene Expression Omnibus (GEO) database, was analyzed to determine common differentially-expressed genes (DEGs) and hub genes between high and low DC environments. The diagnostic value of these genes for IgAN was evaluated using machine learning algorithms and receiver operating characteristic (ROC) curve analysis. The findings were validated through GEO datasets and real-time quantitative PCR (RT-qPCR) in an IgAN mouse model. We identified three small-molecule inhibitors or agonists that effectively modulate the expression of these signature genes. Our results highlight IKZF1, a critical gene expressed by DCs, which plays a pivotal role in IgAN progression. This discovery could guide personalized diagnosis and treatment strategies for IgAN.

Methods

Data pre-processing and differential expression genes analysis

GSE175759 was downloaded from the GEO database (https://www.ncbi.nlm.nih.gov/gds/term=) using the R package GEOquery. The dataset contains 46 IgAN samples and 22 control samples. GSE175759 dataset, which is based on GPL16791. Principal component analysis (PCA) was performed using the "ggplot2" package. The R language "limma conductor" software package was used to perform differential gene analysis. This involved utilizing the "lmFit" function for linear modeling and the "eBayes" function for empirical Bayes statistics. The criteria of $|\log2FC|>1$, $P<0.05$ was used to screen DEGs. The results were visualized in volcano plots based on the "ggplot 2" package, while gene matrix heat maps were drawn using the "Complex Heatmap" package.

Immune cell infiltration analysis by CIBERSORT

The web tool CIBERSORT (http://CIBERSORT.stanford.edu/) was used to calculate immune cell infiltration and explore the immune microenvironment of the disease. CIBERSORT is a common method for calculating immune cell infiltration and estimates the abundance of immune cells by deconvoluting the expression matrix of immune cell subtypes based on the principle of linear support vector regression. The immune cell infiltration of

each sample was calculated using CIBERSORT, and the differences of the abundance of immune cells between the two groups was compared using a Wilcoxon rank sum test, with the screening criterion of $P < 0.05$. Visual analysis was conducted using the "ggplot2" package.

Weighted gene co-expression network analysis

WGCNA was conducted according to previously-described methods [14]. WGCNA was used to analyze the co-expression modules and key genes related to immune cell subsets [14–20]. The parameters were set as follows: $R^2 = 0.9$ and soft-threshold $\beta = 6$. Subsequently, the adjacency matrix was transformed into a topological overlap matrix. A dendrogram was constructed using hierarchical clustering to calculate correlations. Modules were identified using hierarchical clustering (minimum module size = 30). The gene significance, which quantifies the associations of individual genes with the trait of interest, and module membership, which acted as the correlation between the module eigengene and the gene expression profiles, were calculated. The core genes in the module were filtered using a gene significance > 0.5 and a module membership > 0.8.

DCs-associated genes analysis

IgAN patients was stratified into two groups based on the median level of infiltrating, namely, high- and low-abundance of DCs. The R language "limma conductor" software package was used to analyze the differential genes between the two groups of sequencing data, using the screening criteria of $|log2FC| > 1$ and $P < 0.05$. To further analyze the differential expression of DCs-associated genes in IgAN, the R software package "VennDiagram" was used to display the intersecting genes in the form of a Venn diagram.

Gene ontology (GO) functional enrichment and Kyoto encyclopedia of genes and genomes (KEGG) enrichment analysis

An enrichment analysis of the intersecting genes was performed using the R package 'clusterProfiler' to obtain the gene set enrichment results. The minimum gene set five genes and the maximum gene set was 5,000 genes. An adjusted P value < 0.05 was considered statistically significant.

Protein-protein interaction network (PPI)

The target genes were entered into the String platform (https://string-db.org/) to retrieve their reciprocal relatio nships. The organism was set as *Homo sapiens*, and Cytoscape 3.9.0 software was used to visualize the protein-protein interaction (PPI) network. Overlapping targets were also entered into the STRING website to obtain the PPI and Tab Separated Values (TSV) files of the protein interaction network. The downloaded TSV file imported into Cytoscape 3.7.2 software for visualization and screen for the core target with the maximum degree value.

Screening target genes using machine learning analysis

The Least Absolute Shrinkage and Selector Operation (LASSO), Support Vector Machines (SVMs) algorithms and random forest algorithms were utilized in DEGs between DC_high and DC_low to screen the DCs-associated pivot gene. LASSO is a regression analysis algorithm that uses regularization to improve prediction accuracy. The LASSO analysis was undertaken using "glmnet" R package which the response type was set as binomial and the alpha was set as 1. SVM is a supervised machine learning technique widely used for classification and regression analysis. To avoid overfitting, the RFE algorithm is used to select the best genes from the metadata queue. To identify the set of genes with the highest discriminative power, SVM was applied to select the appropriate features. The SVM was performed using "e1071" "kernlab" and "caret" R package. The value of the variable corresponding to the minimum root mean square error (RMSE) represented the number of candidate genes screened. Random forest algorithm is a method with fast training speed and strong anti-overfitting ability, widely used in data preprocessing, classification prediction, and other fields. Random Forest was applied by the R package "randomForest". Finally, the overlapping genes obtained from the three algorithms were used as target genes.

ROC curves of key genes and differential expression analysis

The transcriptome data of the hub genes in diseased and normal tissues were extracted, the ROC curve was analyzed using the "pROC" software package in R software, and the area under the ROC curve (AUC) was calculated to evaluate the clinical efficacy of the hub gene in predicting the presence of disease. The differential expression of intersecting genes at the transcriptional level was then analyzed using a two-sample t-test.

Gene set enrichment analysis of key genes (GSEA)

In this section, IgAN patients was stratified into two groups based on median expression level of IKAROS (IKZF1) and macrophage-expressed gene 1 (MPEG1), namely high and low expression groups. The "DESeq2" package was employed to identify DEGs. After identifying DEGs, we used the c2.cp.kegg.v7.4.symbols.gmt gene set from the MsigDB database of the GSEA (https://www.gsea-msigdb.org/gsea/index.jsp) website as the reference gene set, the potential effect pathway of the intersecting genes was analyzed using the default weighted enrichment statistical method. The screening criteria were set as follows: absolute number of standardized enrichment

scores |NES| >1, (False discovery rate) FDR < 0.25 and *P* value < 0.05 [17, 20, 21].

Correlation analysis

The correlation between key genes and DCs abundance was calculated using Spearman statistical analysis and visualized using the "ggplot2" package.

Construction of miRNA-mRNA networks for Pivot genes

The miRNAs of the pivot genes were predicted using miRanda (http://www.microrna.org/microrna/home.do), miRDB (https://mirdb.org), and TargetScan (https://www.targetscan.org) databases. To improve the accuracy of the predictions, only the miRNAs predicted by all three databases were retained in the analyses.

Animals

Female Balb/C mice (20 ± 2 g, 6 weeks old) and male Wistar rats (200–220 g, 6–8 weeks) were purchased from SPF (Beijing, China) Biotechnology Co. This experimental research plan has been approved by the Animal Ethics Committee of the PLA General Hospital before the start of the experiment. All of the animal care and experimental procedures complied with the guidelines for the Care and Use of Laboratory Animals published by the United States National Institutes of Health (NIH publication, 2011 Revision). The experiments were conducted in compliance with the ARRIVE guidelines and the EU Directive 2010/63/EU for animal research. The sample size calculation was based on the resource equation method [22].

Blood was collected for serum creatinine (SCR) and blood urea nitrogen (BUN) using a Creatinine Assay Kit (C011-2-1) and Urea Assay Kit (C013-2-1) by Nanjing Jiancheng Bioengineering Institute. The levels of urine albumin creatinine ratio (UACR) was detected using commercial kits (C035-2-1, Nanjing Jiancheng, China).

Construction of an IgAN mouse models

Female Balb/C mice (20 ± 2 g, 6 weeks old) were purchased from SPF (Beijing, China) Biotechnology Co. All mice were fed in an environment with constant temperature (20℃), humidity (70%) and alternating day and night. The IgAN mouse model was induced as previously described [23, 24]. Bovine serum albumin (Sigma, USA) in acidified water (800 mg/kg body weight) was administered by gavage every other day. Carbon tetrachloride was dissolved in castor oil (1:5; 0.1 mL) and injected subcutaneously weekly and intraperitoneally (0.08 mL) biweekly. At 6th and 8th weeks, lipopolysaccharide (Sigma, USA) (50 μg) was injected through the tail vein. The IgAN mouse model was established at the end of the 11th week. During the process, IgA deposition in the glomeruli was assessed through direct immunofluorescence to evaluate the establishment of the model. Blood, twenty-four-hour urine samples, and renal tissues were then carefully collected for subsequent experiments.

Construction of an anti-Thy1 nephritis rats

Male Wistar rats (200–220 g, 6–8 weeks) were purchased from SPF (Beijing, China) Biotechnology Co. All rats were fed in an environment with constant temperature (20℃), humidity (70%) and alternating day and night. The anti-Thy1 nephritis model was established in rats by injecting anti-Thy1 antibody (2.5 mg/kg) into the tail vein, while the control equal volume of saline solution. The rats were divided into control group and model group. On the 5th day, the rats were sacrificed and kidney tissues, blood and urine samples were collected.

Lenalidomide treatment in anti-Thy1 nephritis rats

To study Lenalidomide's impact on anti-Thy1 nephritis, rats were administered intraperitoneal injection of Lenalidomide hemihydrate solution (12.5 mg/kg, HY-A0003B, MCE, USA) daily for 5 consecutive days. The control and anti-Thy1 nephritis groups received an equivalent volume of cosolvent. On the 5th day, the rats were sacrificed and kidney tissues, blood and urine samples were collected.

Periodic acid-schiff (PAS)

The kidney samples were fixed in 10% formalin, embedded in paraffin, and sectioned to 4 μm thickness. Sections were stained with PAS to assess glomerular cell proliferation. Images were obtained at 400 × magnification.

Western blotting

A BCA protein quantitation assay (Thermo Fisher Scientific, Waltham, MA, USA) was used to measure the protein levels in tissue or cell lysates and EVs. After denaturation, the proteins were transferred onto nitrocellulose membranes (Roche, Switzerland). The membranes were then blocked with 5% bovine serum albumin (BSA) in Tris-buffered saline with 0.1% Tween 20 detergent (TBST) at room temperature, followed by incubation with antibodies against fibronectin (FN) (1:1000, ab2413, Abcam), GATA3 (1:2000, ab282110, Abacam), PCNA (1:5000, ab92552, Abcam), α-SMA (1:1000, ab7817, Abcam), β-actin (1:10000, 66009-1-Ig, Proteintech).

Cell culture and treatment

The mouse DC2.4 cell line was purchased from Pricella (Wuhan, China) and maintained in RPMI 1640 medium (Corning) supplemented with 10% fetal bovine serum (FBS) and 1% penicillin/streptomycin. Cells were cultured in a humidified incubator at 37 °C with 5% CO_2. Lenalidomide hemihydrate solution was procured from MCE and applied at a concentration of 1 μM.

IKZF1 plasmid and siRNA transfection

Cells were seeded one day prior to transfection. Transfection was performed with siRNA or plasmid when the cell confluence in each well reached approximately 60%. DC2.4 cells were transfected with a vector encoding IKZF1 cDNA ($IKZF1^{ov}$) using EndoFectin Max (GeneCopoeia, Guangzhou, China). Small interfering RNAs targeting mouse IKZF1 were obtained from GenePharma (Shanghai, China). RNA and cells were harvested 24 h post-transfection. In intervention experiments, LPS treatment was applied 12 h after transfection.

Immunofluorescence (IF) and immunohistochemistry (IHC) staining

IF and IHC staining was performed as described previously [25, 26]. The primary antibodies used were Kidney Injury Molecule-1 (KIM-1) (1:400, AF1817, R&D), FN (1:200, ab2413, Abcam), CD103 (1:100, ab224202, Abcam), IKZF1 (1:100, 66966-1-Ig, Proteintech), GATA3 (1:2000, ab282110, Abacam), PCNA (1:500, ab92552, Abcam), α-SMA (1:100, ab7817, Abcam), Collagen-I (1:100, ab270993, Abcam), CD4 (1:2000, ab237722, Abcam), Anti-Ikaros (1:1000, ab300405, Abcam) and CD68 (1:100, ab125212, Abacam). The tissue sections were imaged using Olympus confocal fluorescence microscopy.

RT-qPCR

Total RNA was extracted from cells or kidney tissue using TRIzol reagent (Invitrogen, location). SuperScript III First-Strand Synthesis System (Applied Biosystems, USA) was used to synthesize complementary DNA. The qPCR system was established according to the manufacturer's instructions using the SYBR Select Master Mix (Thermo Fisher Scientific, location). The primer sequences are listed in Table S1.

Multiplex immunohistochemical (mIHC) staining

The tissue microarray was stained using the PANO 7-plex IHC kit (cat 0004100100, Panovue, Beijing, China) following the standard protocol. Slides were deparaffinized in xylene, rehydrated, and washed in tap water, then subjected to antigen retrieval. Tissue areas were marked, and protein blocking was performed with Antibody Diluent/Block (CST). Antigens were labeled sequentially, starting with primary antibody incubation: Anti-Ikaros (1:1000, ab300405, Abcam) and CD103 (1:100, ab224202, Abcam). Afterward, secondary antibody incubation and TSA visualization were performed, followed by labeling with the next antibody. Primary antibodies were incubated for 1 h at room temperature, followed by incubation with Opal Polymer HRP at 37 °C for 10 min. TSA visualization was carried out using the PANO 7-plex IHC kit, with microwave treatment to remove the Ab-TSA complex during antigen retrieval. The slides were counterstained with DAPI for 5 min and mounted in an antifade medium. Slides were scanned using the Olympus VS200 MTL (Olympus, Germany).

Flow cytometry

Single-cell suspensions of DC 2.4 or kidney cells were incubated with surface marker antibodies at 4 °C for 30 min. The cells were then fixed and permeabilized, followed by intracellular antibody Ikaros (Abcam, #ab300405) staining for 30 min at 4 °C. After each staining step, the cell suspension was washed twice. Data acquisition was performed using a BD LSR Fortessa TM cytometer, and the analysis was conducted with BD FlowJo TM v10.6.2 software. The following reagents and antibodies were used: live-dead-Zombie (BioLegend, #423106), CD11c-PE (BioLegend, #558079), MHC II-APC (BioLegend, #107614), CD45-APC(BioLegend,#202216), CD11b/c-PE (BioLegend, #201817), CD103-FITC (BioLegend, #205505), Abflo594 conjugated Goat Anti-Rabbit IgG (ABclonal, #AS086) and isotype controls.

Statistical analysis

The data were analyzed using GraphPad Prism 7.0, and all group data are presented as the mean ± SEM. The statistical analyses were conducted using Student's t-test or one-way analysis of variance (ANOVA). When the ANOVA showed a significant difference, post-hoc analysis between group means was performed using Tukey's. Statistical significance was set at $P < 0.05$. The data from more than 3 independent experiments.

Results

Immune cell infiltration in the renal interstitial tissues of IgAN

We analyzed differential gene expression in 46 IgAN samples and 22 controls. PCA of the 68 samples clearly separated the IgAN group from the control group (Fig. S1). A total of 474 DEGs were identified, including 312 upregulated and 162 downregulated genes in IgAN renal interstitial tissues compared to healthy controls (Fig. S2A). Genes related to leukocyte migration, inflammation, antigen processing, and presentation were elevated in IgAN samples, while lipid metabolic process genes were downregulated (Fig. S2B). CIBERSORT analysis revealed that M1 macrophages, resting DCs, resting mast cells, neutrophils, naive B cells, T follicular helper (Tfh) cells, and regulatory T cells (Tregs) were the predominant immune cells associated with renal interstitial infiltration in IgAN patients (Fig. 1A). WGCNA identified modules of highly interconnected genes. A soft threshold of six was selected to ensure a scale-free network (scale-free $R^2 = 0.9$, Fig. 1B-D). Modules with high similarity

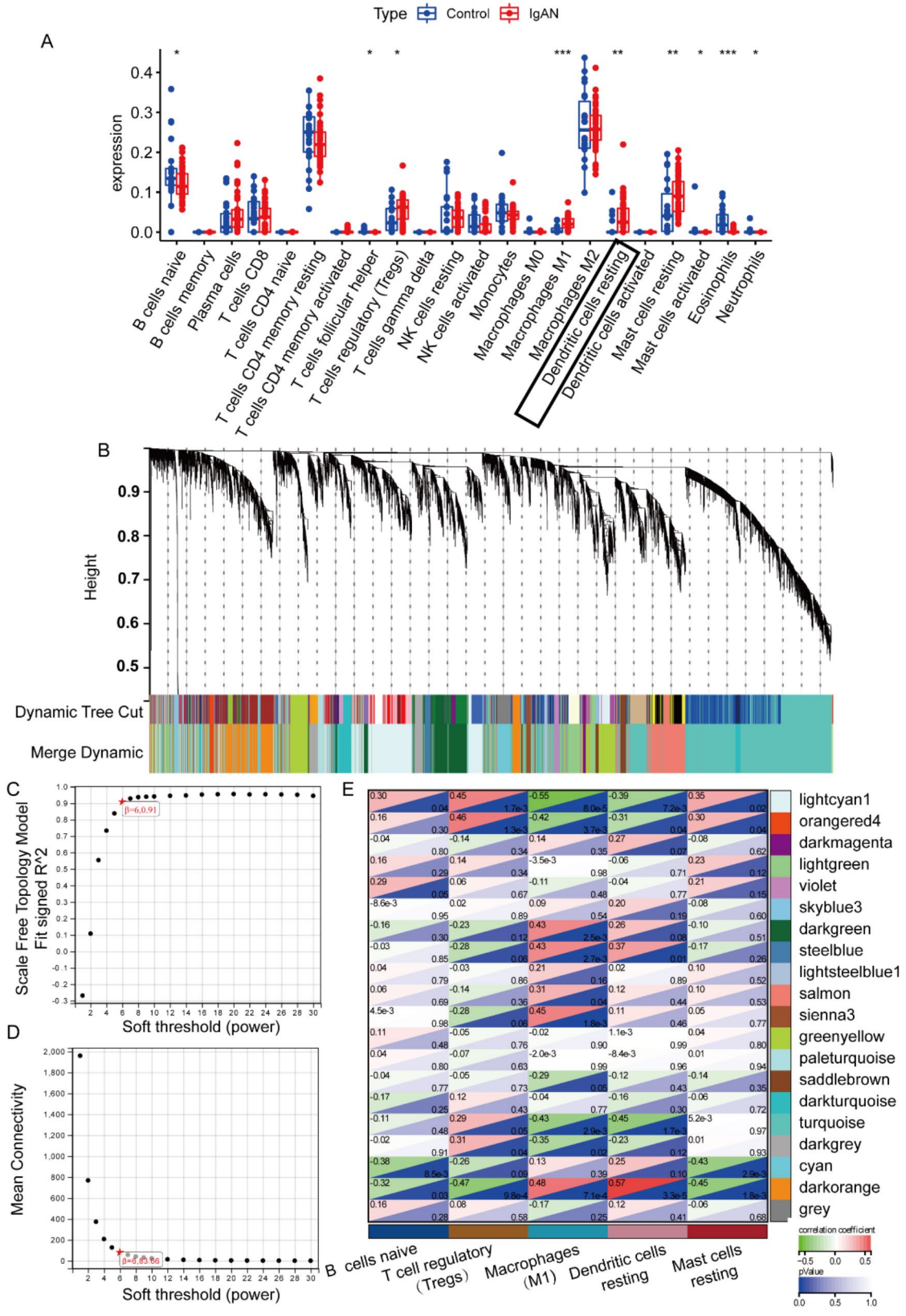

Fig. 1 Analysis of immune cells infiltration and identification of immune cells-associated key modules based on WGCNA analysis. (**A**) Violin plot of the immune cell proportions by CIBERSORT analysis. (**B**) The clustering of genes into distinct groups. (**C**-**D**) The characteristics of the network architecture were established using distinct power values; the correlation between power and average connection is shown. (**E**) Module-trait relationship between clustered modules and immune cells type. Each row corresponds to a module Eigen gene, and each column to the type of immune cells

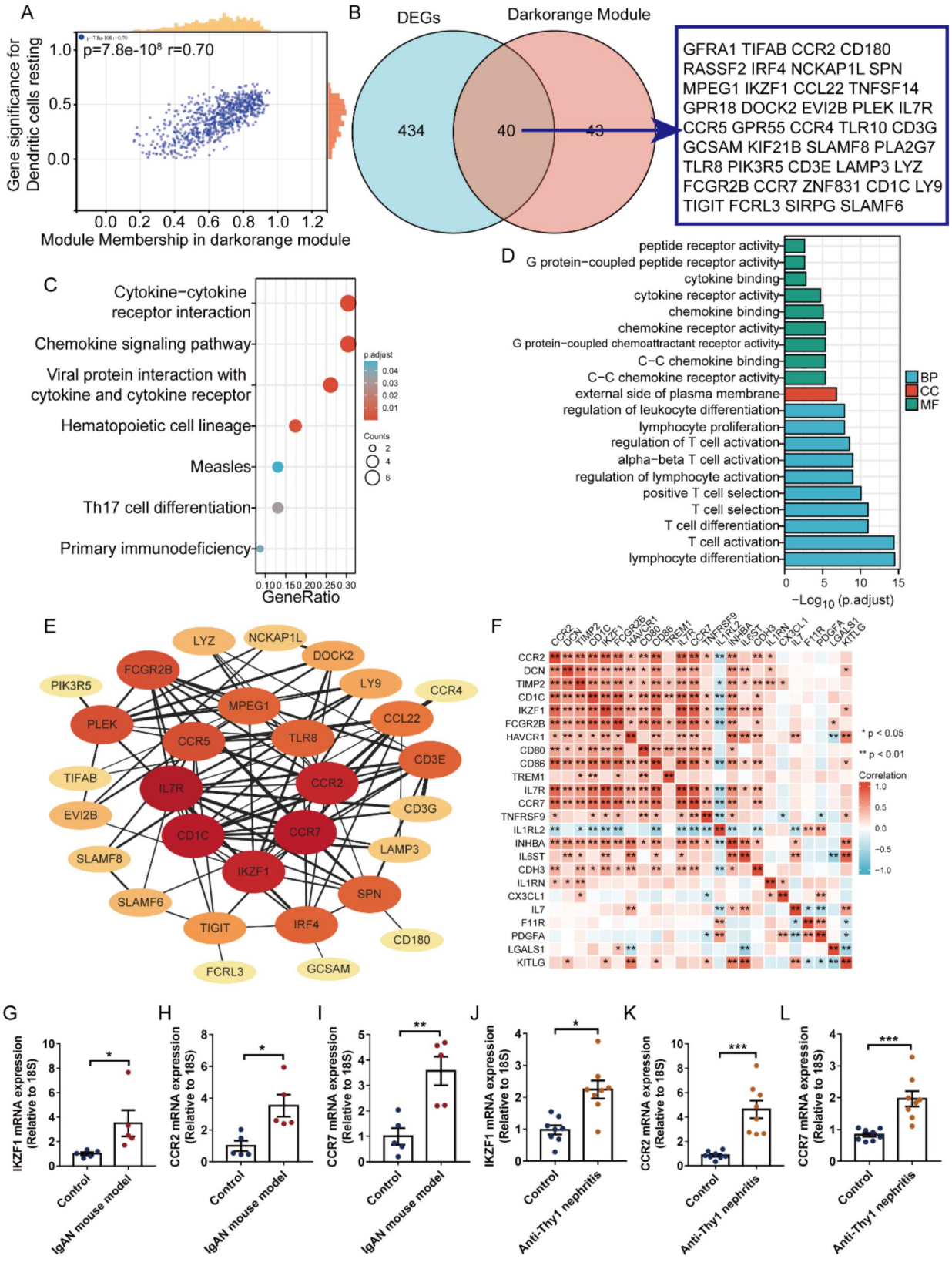

Fig. 2 (See legend on next page.)

(See figure on previous page.)

Fig. 2 Identification and validation of dendritic cells-related hub genes screened by WGCNA for IgAN. (**A**) Scatter plots of the GS score and MM for Dendritic cells resting in the darkorange modules. (**B**) Venn diagram showed intersected genes between WGCNA module (Dendritic cells and darkorange) genes and DEGs (IgAN vs. Control). (**C**) The KEGG pathway enrichment analysis and (**D**) the GO (biological process (BP), molecular function (MF), Cellular Component (CC)) enrichment analysis of the intersected genes. (**E**) The PPI network of the intersected genes. (**F**) The correlation among intersected genes. (**G**-**L**) mRNA expression levels of IKZF1, CCR2, and CCR7 in IgAN mouse model (**G**-**I**, $n=5$) and anti-Thy1 nephritis rats (**J**-**L**, $n=8$) models were detected by RT-qPCR. Results are presented as the mean values (± SEM), $^{*}P<0.05$, $^{**}P<0.01$, $^{***}P<0.001$ versus Control

were merged based on the gene cluster dendrogram (Fig. 1E). The darkorange module, strongly correlated with resting dendritic cells ($r=0.57$, $P<0.001$; Fig. 1E), was further analyzed.

Identification and validation of dendritic cells-related hub genes for IgAN

We visualized the correlation between resting DCs and darkorange module (Fig. 2A). After that A Venn diagram confirmed the presence of DEGs related to the resting DCs (Fig. 2B). The chemokine signaling pathway and Th17 cell differentiation were identified as underlying biological functions of the DEGs using KEGG (Fig. 2C). Cytokine binding and chemokine receptors were identified using the GO enrichment analysis (Fig. 2D). PPI network analysis demonstrated interactions among IKZF1, CCR2, CCR7, CCL22, TLR8, MPEG1, CCR5, IL7R (Fig. 2E). Strong positive associations were identified between the expression levels of the CD1C, IKZF1, CCR2, CCR7 and others (Fig. 2F). To validate the expression patterns of key genes, we successfully established both the IgAN mouse model and the anti-Thy1 nephritis rat model. The success of model establishment was confirmed by evaluating the level of SCR, BUN, UACR, and the deposition of IgA and Thy1 in the mesangium (Fig. S3). The expression of IKZF1, CCR2, and CCR7 were significantly upregulated in the IgAN mouse model and anti-Thy1 nephritis rats using RT-qPCR (Fig. 2G-L).

Identification and function enrichment of DEGs for IgAN based on DCs abundance

To identify DEGs associated with DCs, we conducted a comparative analysis of gene expression between high- and low-dendritic cell subgroups. We first estimated DC abundance in each sample using the CIBERSORT deconvolution method. Then, we performed differential expression analysis. A total of 325 DEGs were identified, including 131 downregulated and 194 upregulated genes (Fig. 3A). To investigate significant differences between the subgroups, we generated a heat map (Fig. 3B). The DEGs from the high- and low-dendritic cell abundance groups were intersected with those from IgAN versus control analysis to identify DEGs related to DC phenotypes in IgAN. We found 103 upregulated intersections (Fig. 3C) and two downregulated intersections (Fig. 3D). KEGG pathway analysis revealed associations with chemokine signaling, T-cell receptor signaling, Th17 cell differentiation, and the intestinal immune network for IgA production (Fig. 3E). GO enrichment analysis showed that these intersections were primarily enriched in cell surface receptor signaling, leukocyte activation, and lymphocyte activation (Fig. 3F).

IKZF1 are effective diagnostic markers of IgAN based on machine learning algorithm

To identify key genes associated with IgAN and DCs function, this study used three machine learning methods: SVM, LASSO, and Random Forest. LASSO regression analysis identified eight key DEGs (TREML2, MPEG1, LILRA4, IKZF1, GAPT, CD1E, C10orf105, ARC) (Fig. 4A). SVM screening revealed 13 key DEGs (MPEG1, IKZF1, XCR1, CD3G, TREML2, DOCK2, IL7R, TLR10, LILRA4, GRIN2A, CD1E, GAPT, SLAMF6) (Fig. 4B). The Random Forest algorithm selected 11 key DEGs with importance scores > 0.5(CD3G, IKZF1, DOCK2, XCR1, CCR2, ZNF831, MS4A1, MPEG1, TLR10, SLCO5A1, CCR7) (Fig. 4C). A Venn diagram analysis of the results from all three methods identified two overlapping genes: MPEG1 and IKZF1 (Fig. 4D). These two genes showed significantly higher expression in IgAN samples compared to controls (Fig. 4E) and demonstrated high diagnostic efficacy (AUC > 0.75) (Fig. 4F).

Additionally, we performed a correlation analysis between the identified marker genes and DCs. The results revealed that IKZF1 and MPEG1 were significantly and positively correlated with DCs (Fig. 4G and Fig. S4A), suggesting that these genes may functionally interact to influence DC activity in IgAN. Furthermore, the high-IKZF1 subgroup was enriched in pathways related to cell adhesion molecules, chemokine signaling, cytokine–cytokine receptor interactions, hematopoietic cell lineage, and natural killer cell-mediated cytotoxicity (Fig. 4H). In contrast, the high-MPEG1 subgroup exhibited greater enrichment in pathways associated with cell adhesion molecules, chemokine signaling, cytokine–cytokine receptor interactions, graft-versus-host disease, and hematopoietic cell lineage (Fig. S4B). By integrating gene-miRNA interaction data from the miRanda, miRDB, and TargetScan databases, we constructed a comprehensive miRNA regulatory network for core genes. This analysis identified both MPEG1 and IKZF1 as targets of multiple miRNAs, including miR-33a-3p and miR-548p (Fig. S4C).

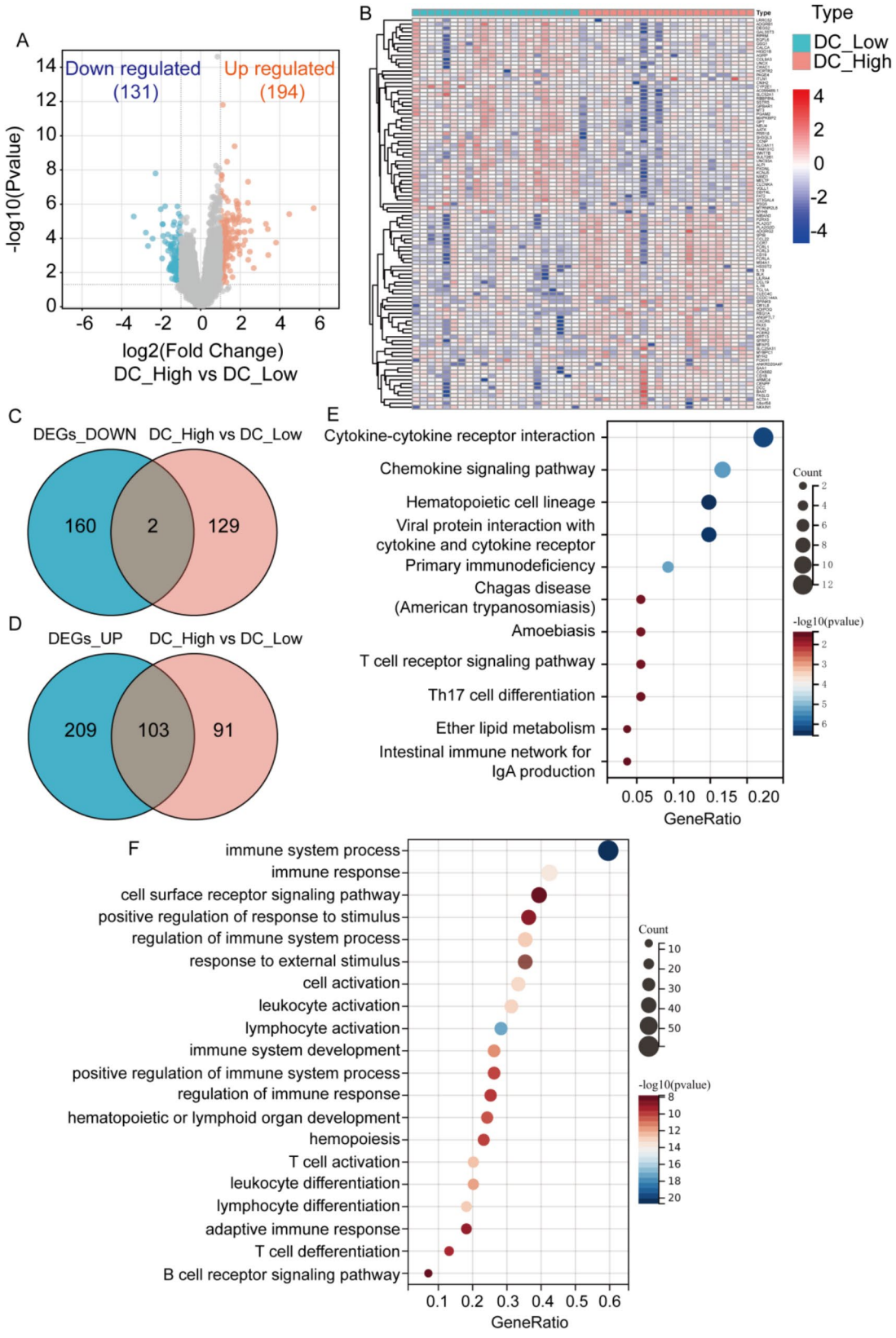

Fig. 3 Identification and function enrichment of high-low DCs DEGs for IgAN. (**A**) A volcano plot of DEGs between high-DCs and low-DCs. (**B**) A heatmap of DEGs between high-DCs and low-DCs. (**C**-**D**) Venn diagram showed DEGs associated with DCs-associated DEGs were found. (**E**) The KEGG pathway enrichment analysis and (**F**) the GO (BP) enrichment analysis of the intersected targets

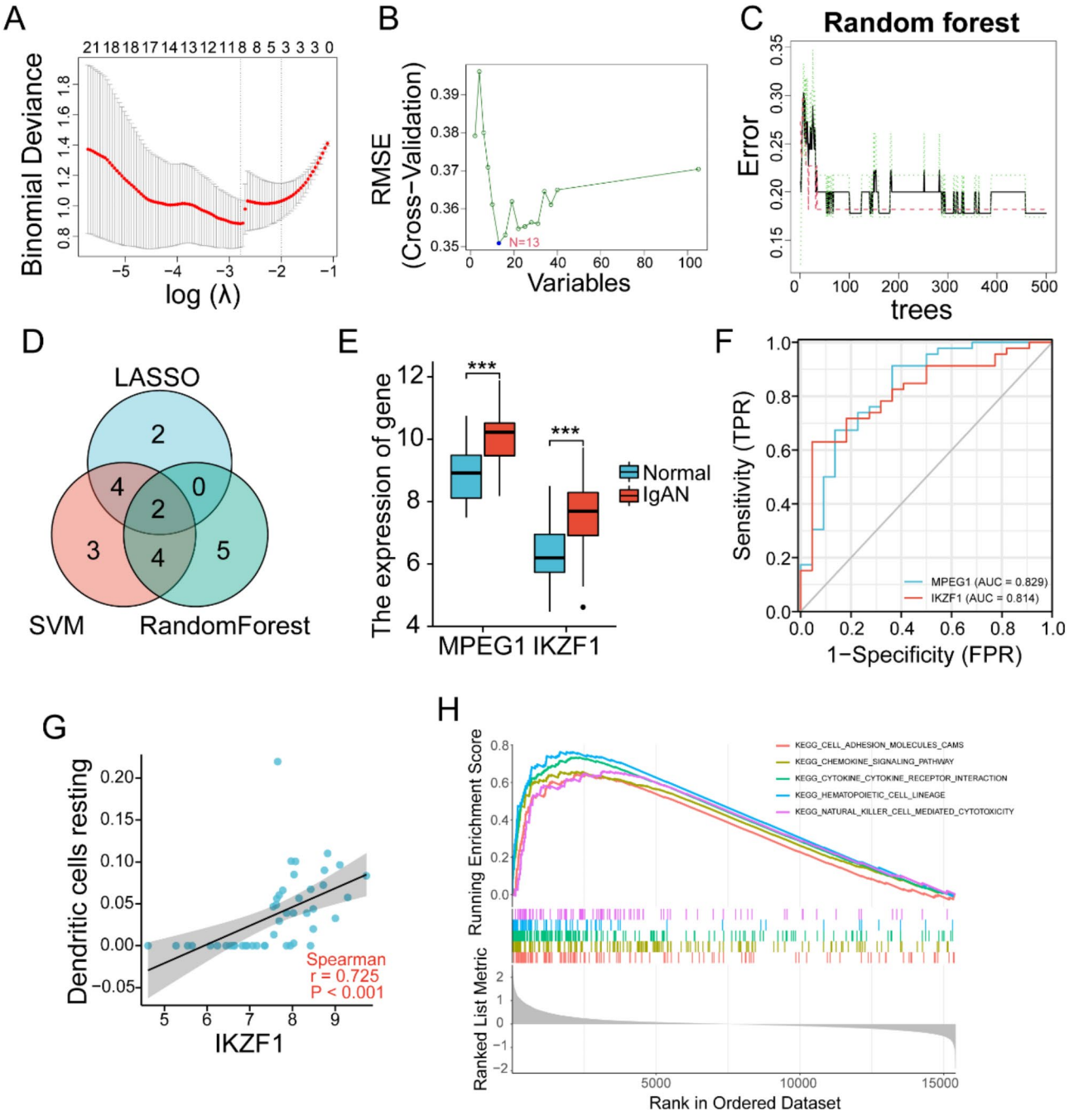

Fig. 4 Identification the characteristic genes of high-low DCs DEGs for IgAN by machine learning algorithm. (**A**) Eight characteristic genes of LASSO. (**B**) Thriteen characteristic genes of SVM. (**C**) Eleven characteristic genes of Random Forest. (**D**) Venn diagram showing the optimal target genes. (**E**) Expression of IKZF1 and MPEG1 in GSE175759. (**F**) ROC curve of IKZF1 and MPEG1 in GSE175759. (**G**) The scatter plot shows the correlation between the proportion of dendritic cells and IKZF1 expression. (**H**) KEGG enrichment analysis using GSEA for IKZF1. ***$P < 0.001$ versus Normal

Expression and role of IKZF1^{+}DCs in IgAN mouse model and anti-Thy1 nephritis model

To evaluate the expression patterns of IKZF1 and infiltration patterns of CD103^{+} DCs in IgAN, we established an IgAN mouse and an anti-Thy1 nephritis rat model. Both models were successfully developed, as confirmed by preliminary experiments (Fig. S3). PAS staining demonstrated significant intraglomerular cell proliferation in the IgAN mouse model compared to the control group, with mild tubular injury (Fig. 5A). FN and KIM-1 staining revealed marked intraglomerular cell proliferation and renal tubular injury, along with increased FN expression in both glomeruli and interstitium in IgAN mouse tissues (Fig. 5B-C). Western blot analysis

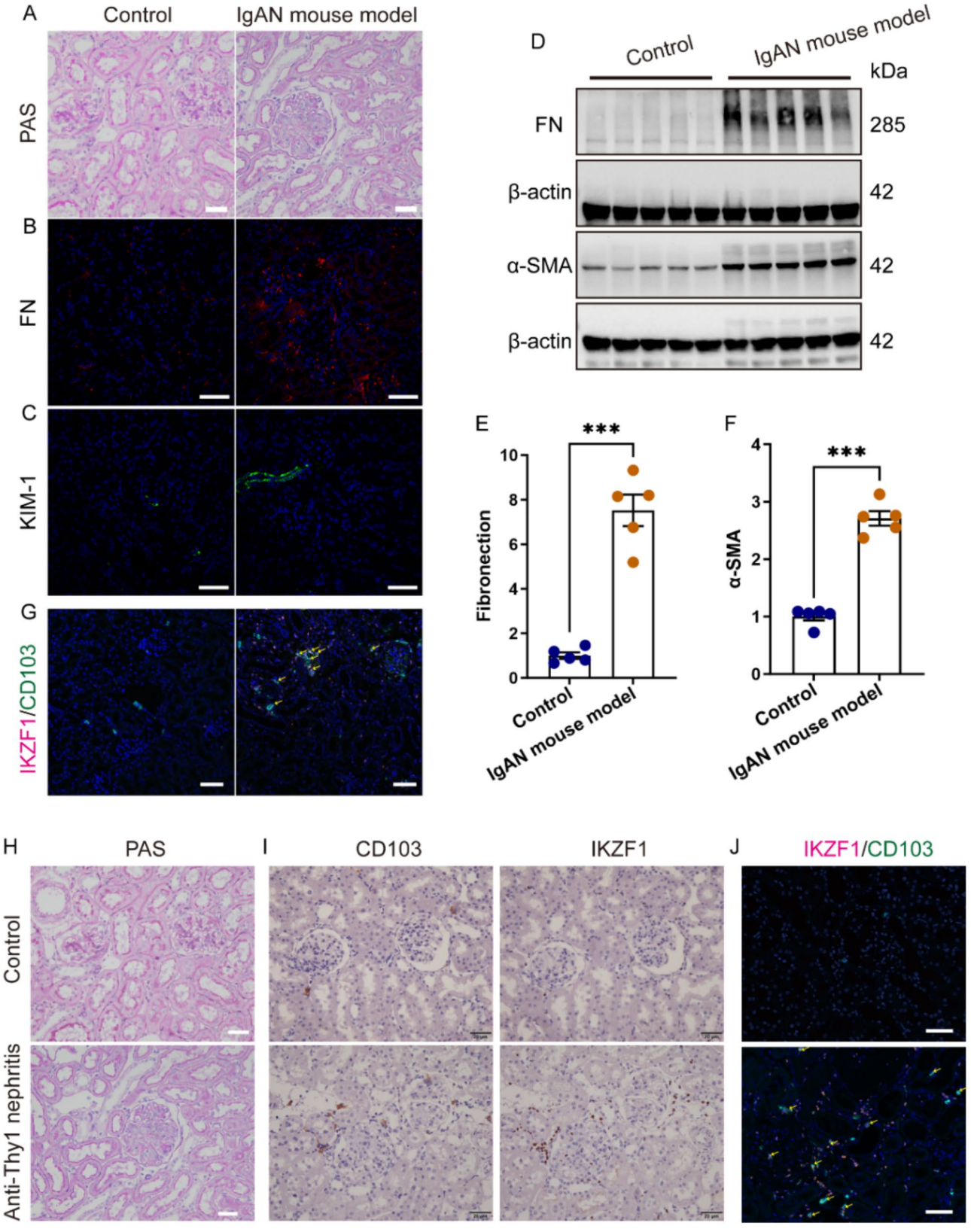

Fig. 5 (See legend on next page.)

(See figure on previous page.)

Fig. 5 Expression and role of IKZF1^{+}DCs in IgAN mouse and Anti-Thy1 nephritis rats. (**A**) PAS shown the pathological features of kidney injury in IgAN mouse model (Scale bar = 20 μm). (**B**-**C**) Immunofluorescence images showed the staining for FN (red) (**B**) and KIM-1 (green) (**C**) in kidney tissues between IgAN mouse model and control groups (Scale bar = 50 μm). (**D**-**F**) Western blotting and quantification of the expression of the FN and α-SMA. (**G**) Immunofluorescence images showed the staining for dendritic cell (CD103, red) and IKZF1 (green) in kidney tissues between IgAN mouse model and control groups (Scale bar = 50 μm). (**H**) PAS staining shown the pathological features of kidney injury in anti-Thy1 nephritis rats (Scale bar = 20 μm). (**I**) Immunohistochemical staining of dendritic cell (CD103) and IKZF1 in kidney tissues between between anti-Thy-1 nephritis and control groups (Scale bar = 20 μm). (**J**) mIHC images showed the staining for dendritic cell (CD103, green) and IKZF1 (red) in kidney tissues between between anti-Thy-1 nephritis and control groups (Scale bar = 50 μm). Data are presented as means ± SEM, $n = 5$; $^{***}P < 0.001$

confirmed elevated FN and α-SMA expression in the IgAN mouse model (Fig. 5D-F and Fig. S6). To investigate IKZF1 expression in DCs, we analyzed the proportion of IKZF1^{+}CD103^{+} DCs using mIHC co-staining. Results showed a significantly higher proportion of IKZF1^{+}CD103^{+} DCs in the renal interstitium of the IgAN mouse model compared to the control group (Fig. 5G). Consistent with kidney injury in the IgAN mouse model, mesangial cell proliferation and accumulation of mesangial matrix were observed (Fig. 5H). Immunohistochemical staining further revealed an increased number of IKZF1^{+}CD103^{+} DCs in rats from the anti-Thy1 nephritis group (Fig. 5I-J).

IKZF1 regulates the DCs function

To investigate the functional changes in DCs regulated by IKZF1, we conducted experiments involving the knockdown or overexpression of the IKZF1 gene in DCs, followed by treatment with Lenalidomide. DC2.4 cells were transfected with IKZF1 siRNA (siIKZF1), IKZF1 overexpression plasmid (IKZF1^{ov}) or their respective negative controls (Control). RT-qPCR results showed that IKZF1 mRNA expression was significantly reduced in the siIKZF1 group and increased in the IKZF1^{ov} group compared to with the levels in the control group (Fig. 6A-B). RT-qPCR was conducted and demonstrated that the expression of TNF-α and IL-1β were increased in IKZF1^{ov} group; however, when IKZF1 was overexpressed alongside Len treatment, this expression of inflammatory cytokines was reduced (Fig. 6C-D). Morever, the results indicated that antigen presentation molecules MHC II and inflammatory cytokines (TNF-α and IL-1β) were upregulated in LPS compared to the control group. However, overexpressing and inhibiting and IKZF1 respectively strengthened and reversed the effects of the LPS treatment (Fig. 6E-H). As above, it suggested that IKZF1 promote inflammation by producing pro-inflammatory factors and antigen presentation in DCs, and could be rescued by siIKZF1 or Len treatment under LPS conditions.

Lenalidomide treatment relieve anti-Thy1 nephritis kidney injury

Since the IKZF1 increases susceptibility to IgAN, we sought to ascertain whether the elimination of IKZF1 conversely attenuates the progression of renal injury. Lenalidomide (Len) is an active immunomodulator and a ligand of the ubiquitin E3 ligase cereblon (CRBN), capable of selectively ubiquitinating and degrading the lymphoid transcription factor IKZF1 via the CRBN-CRL4 ubiquitin ligase. Underwent anti-Thy1 antibody injection, mice were treated for consecutive 5 days (Fig. 7A). Gratifyingly, BUN, SCR, and UACR were all significantly lower in the Len treatment group compared to the other two groups (Fig. 7B-D). Subsequent PAS staining showed a significant reduce in nucleus number per glomerular in all Len treated mice as compared to their controls (Fig. 6E-F). Then we use immunohistochemical staining (Fig. 7G) and western blotting (Fig. 7H and Fig. S5A-B) with GATA3 and PCNA, associated with activation of mesangial cells and abnormal proliferation and extracellular matrix deposition, to verify the effect of Len on cell proliferation. As Fig. 7G-H shows GATA3 and PCNA-positive cells increased in the anti-Thy1 nephritis group and decreased after Len treatment. And western blotting analysis further confirmed attenuated α-SMA and FN expression after being treated with Len treatment (Fig. 7H and Fig. S5C-D), indicated Len treatment could reduce cell proliferation, cell–matrix accumulation, and fibrosis. Furthermore, α-SMA expression was remarkably declined in Len treatment group compare to the other two groups (Fig. 7I-J).

Lenalidomide, as an IKZF1-targeting molecular glue degrader, suppresses immune cell infiltration

Next, we made continuing efforts to explore the effect of Len, as IKZF1 degrader, on the immunoregulation in anti-Thy1 nephritis by assessing multiple immune cells infiltration. To validate the efficacy of Len, we performed immunohistochemical staining of IKZF1 in the kidney (Fig. S7). The results demonstrated the expression of IKZF1 reduced after Len treatment in anti-Thy1 nephritis rats. We then measured the number of IKZF^{+}CD103^{+}DCs by mIHC staining, showed that the Len treatment mice had fewer IKZF1^{+}CD103^{+} DCs per HPF area as compared to the anti-Thy1 nephritis mice (Fig. 8A-B). Consistent with the aforementioned results, after Len treatment, the proportion of IKZF1^{+}CD103^{+} DCs among CD11b/c immune cells decreased from 0.56 to 0.084% (Fig. 8C, D). Moreover, compare to the anti-Thy1 nephritis group, CD103, CD4 and CD68 positive rate both lessened in Len treatment group which

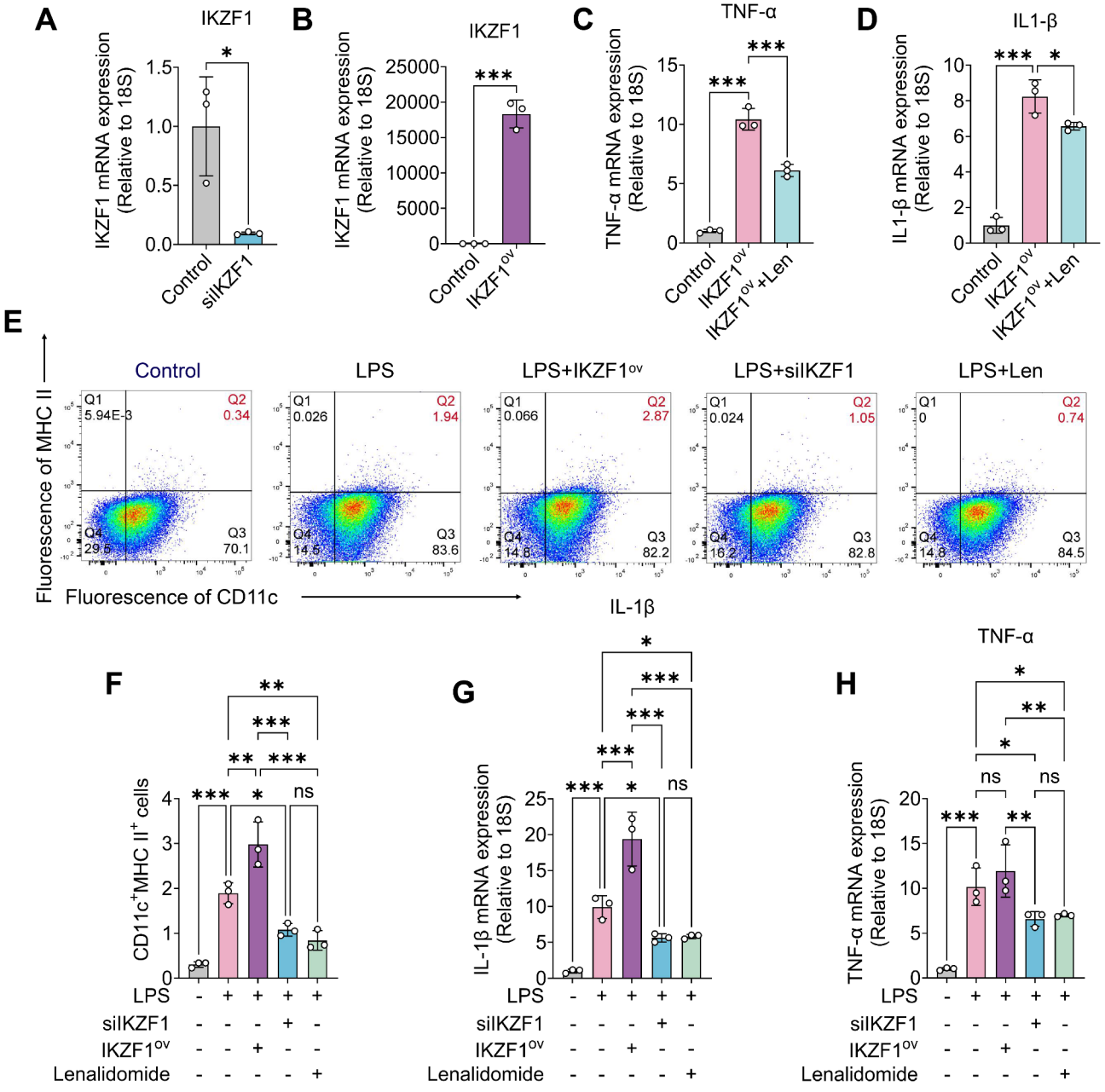

Fig. 6 IKZF1 regulates the DCs function. **(A-B)** IKZF1 was knocked down and overexpressed at the mRNA level in DC2.4 cells. **(C-D)** RT-qPCR analysis of TNF-α **(C)** and IL-1β**(D)** mRNA expression on podocyte under IKZF1^{ov} and IKZF1^{ov} with Lenalidomide treatment. **(E-F)** Percentage of MHC II^{+}CD11c^{+} DCs. **(G-H)** mRNA expression levels of IL-1β**(G)** and TNF-α **(H)** were detected using qRT-PCRin DC2.4 cells under various conditions, including LPS stimulation alone, LPS combined with siIKZF1 or IKZF1 overexpression, and Lenalidomide treatment.Data are presented as means ± SEM, n = 3; *$P < 0.05$, **$P < 0.01$, ***$P < 0.001$

indicates Len treatment inhibit CD103^{+} cells, CD4^{+} T cells and CD68^{+} macrophage cells infiltration in anti-Thy1 nephritis (Fig. 8E-J). Simultaneously, we detected several chemokine receptors expression which found out anti-Thy1 nephritis was highly correlated with the expression of CCR2, CCR5, CCR7 and IL7R which significantly promoted their expression as compare to control group (Fig. 8K-N). And as expect, Len treatment have alleviated those chemokine receptors expression as compare to anti-Thy1 nephritis group. Collectively, Len could regulate several immune cells infiltration and restrain anti-Thy1 nephritis induced chemokine receptors represented by the CCR family.

Discussion

IgAN is the most prevalent primary glomerulonephritis worldwide and is a leading cause of renal failure [27]. Approximately 20–40% of patients experience

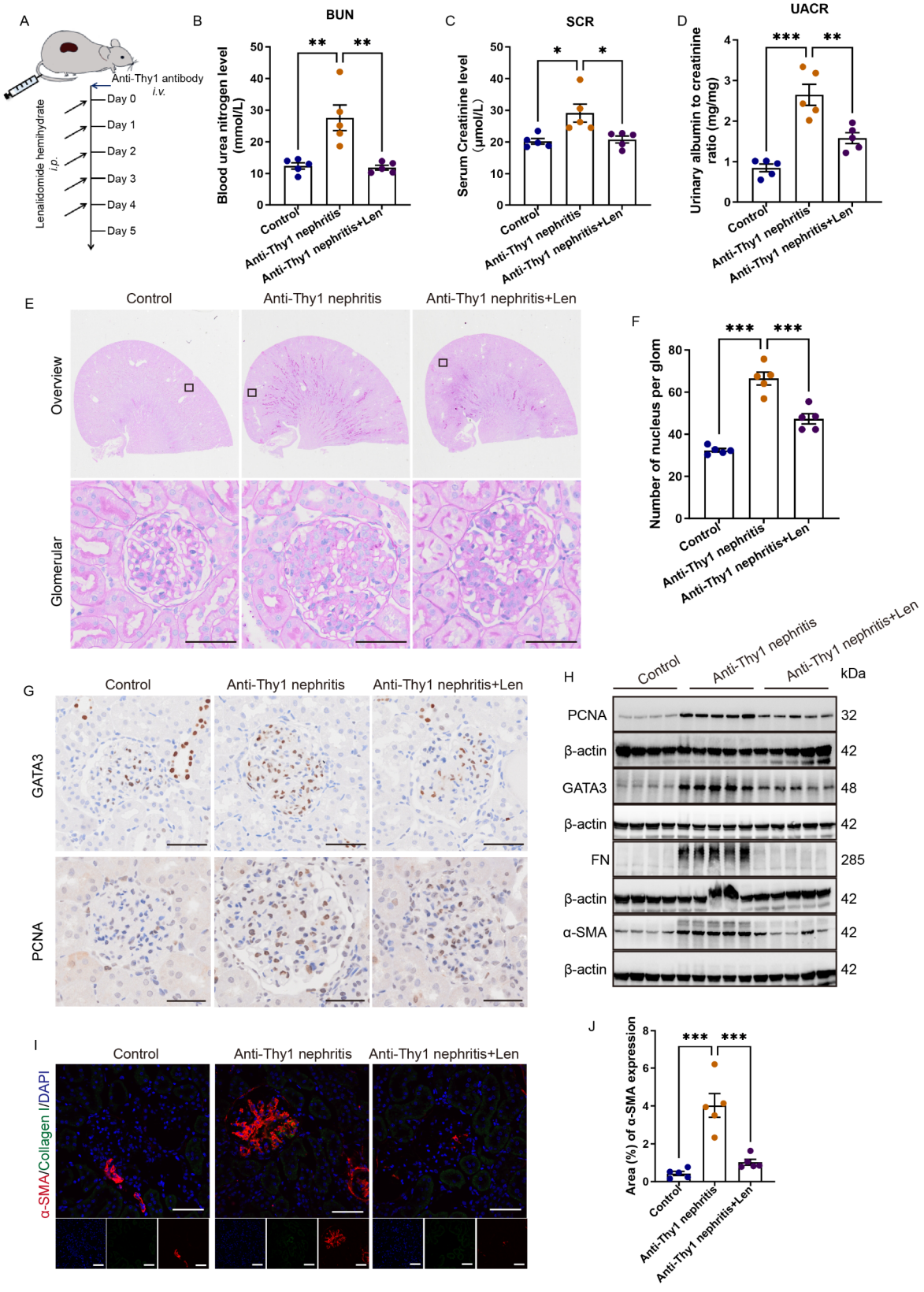

Fig. 7 (See legend on next page.)

(See figure on previous page.)

Fig. 7 Lenalidomide treatment relieve anti-Thy1 nephritis kidney injury. **(A)** Schematic illustration Lenalidomide (Len) administration for anti-Thy1 rats. Male rats were administered intraperitoneal injections of normal saline and 12.5 mg/kg Len for 5 days. **(B-D)** Renal function parameters BUN, SCR and UACR were assessed. **(E)**Representative kidney images following PAS staining after the Len treatments. **(F)** Quantification of the number of nuclei per glomerulus after Len treatment in **(E)**. **(G)** Immunohistochemical staining of cell proliferation markers GATA3 and PCNA in the kidney from anti-Thy1 nephritis rats. **(H)** Western blotting of the mesangial cell proliferation marker PCNA, GATA3, FN and α-SMA. **(I-J)** Representative immunofluorescence staining and quantification of α-SMA images in kidneys after Len treatment. α-SMA (red), Collagen-I (green) and DAPI (nuclear; blue). Data are presented as means ± SEM, n = 5; **P*< 0.05, ***P*< 0.01, ****P*< 0.001. Scale bar = 50 μm

progression to kidney failure within 20 years of diagnosis, resulting in an average reduction in patient life expectancy by approximately 10 years [28]. The pathogenesis of IgAN involves a series of four sequential processes, known as the "four-hit hypothesis" [29]. This hypothesis suggests that the pathogenesis of IgAN begins with elevated levels of abnormally glycosylated galactose-deficient IgA1 (gd-IgA1) in circulation, leading to the formation of immune complexes with anti-gd-IgA1 antibodies and their subsequent deposition in the glomerular mesangium, ultimately resulting in kidney inflammation and injury [30].

We analyzed DEGs in the renal interstitial tissues of individuals with IgAN and healthy controls, constructing a differential expression profile with 312 upregulated and 162 downregulated genes. Subsequent bioinformatics analyses elucidated the pathogenic roles of these genes in IgAN. Our findings showed that these genes are primarily involved in inflammatory processes, such as leukocyte migration and antigen presentation. A growing body of clinical, biochemical, and genetic evidence consistently supports the involvement of innate and adaptive immunity, as well as immune microenvironment homeostasis, in the intricate pathogenic process of IgAN [6, 31]. The renal immune microenvironment involves an array of immune cells (including neutrophils, dendritic cells, macrophages, B lymphocytes, and T lymphocytes) and resident renal cells (including glomerular mesangial cells and renal tubular epithelial cells) [32]. These cells secrete cytokines, chemokines, adhesion molecules, and complement factors that play pivotal roles in the progression of IgAN.

To clarify the differences in immune cell types in IgAN, the CIBERSORT algorithm was used to analyze the infiltration of 22 types of immune cells in renal interstitial tissue in the setting of IgAN [33]. It was determined that the infiltrations of naïve B cells, Tfh cells, Tregs, and DCs significantly increased. Du et al. reported an increase in the infiltration of $CD4^+$T and B cells into the kidneys of patients with IgAN [34]. B cells exhibit increased differentiation and activation capacities in patients with IgAN [34]. In the presence of microbial pathogens or food antigens, the activation of DCs triggers T-cell-dependent B-cell differentiation into IgA-secreting cells. Based on previous studies, DCs are essential for initiating adaptive immunity and bridging the gap between innate and adaptive immune responses [35, 36]. Therefore, this study investigated the role of DCs and their associated genes in IgAN.

DCs are crucial antigen-presenting cells that play a pivotal role in initiating immune responses against acquired immunity [37, 38]. DCs are not only more potent than other antigen-presenting cells but also possess the unique ability to activate naive T cells, induce T cell differentiation through various co-stimulatory factors, and promote immune tolerance in response to environmental stimuli. Under steady-state conditions, DCs are predominantly localized within the secondary lymphoid organs and tissues. Following an inflammatory stimulus, DCs migrate to the site of inflammation, where they are activated and induce T-cell polarization [6]. Previous studies have reported that DCs are pathogenic in various kidney diseases, suggesting that they are important for the initiation and progression of these diseases. DCs are pathogenic in murine models of chronic kidney diseases including experimental nephrotoxic nephritis, glomerulonephritis and lupus nephritis, suggesting an important role in the initiation and progression of acute and chronic kidney disease [39]. Esteve et al. demonstrated an increased proportion of DCs in the setting of IgAN, which corresponds with the findings of a previous study regarding immune cell infiltration [6]. Liu et al. reported that patients exhibit proteinuria, a lower estimated glomerular filtration rate, tubule atrophy, and tubule interstitial sclerosis when DCs infiltrate the tubulointerstitium [40]. Renal DCs intricately establish a complex network within the tubule interstitium, wherein they continuously phagocytose antigens and subsequently present them to T lymphocytes. In progressive kidney disease, the rate of DCs migration to sites of injury increased [41].

Previous studies have reported that $CD103^+$ DCs represent a distinct subset of DCs found in non-lymphoid organs, such as the kidney and intestine [42]. In the current study, immunofluorescence staining revealed that the proportion of $IKZF1^+CD103^+$DCs in the renal interstitium of IgAN model was increased, and co-staining with FN and KIM-1 suggested renal tubular injury in this region (Fig. 7). This result is consistent with previous findings, suggesting the involvement of these genes in the progression of IgAN. $CD103^+$DCs have been reported to play a crucial role in various chronic kidney diseases. Zhang et al. demonstrated that treatment with mesenchymal stem cells (MSC) reduces the infiltration of $CD103^+$DCs, leading to the amelioration of inflammation

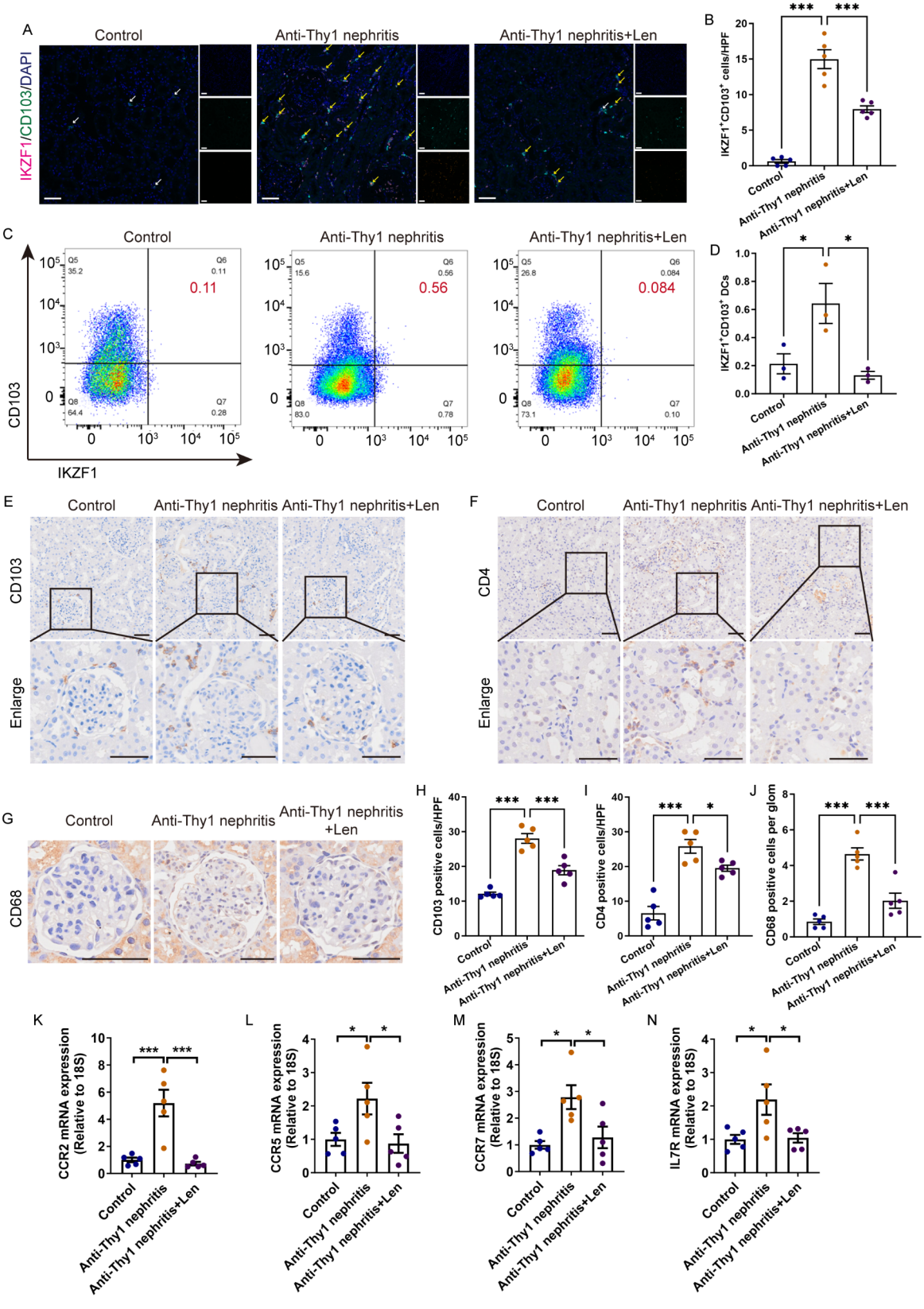

Fig. 8 (See legend on next page.)

(See figure on previous page.)

Fig. 8 Lenalidomide, as an IKZF1-targeting molecular glue degrader, suppresses immune cell infiltration. (**A**) mIHC images showed the staining for dendritic cell (CD103, green) and IKZF1 (red) in kidney tissues in anti-Thy-1 nephritis after Len treatment. (**B**) Quantification of IKZF1$^+$CD103$^+$ DCs in (**A**). (**C**-**D**) Percentage of IKZF1$^+$CD103$^+$ DCs. (**E**-**J**) Representative images and quantitative analyses of CD103 (**E**, **H**), CD4 (**F**, **I**) and CD68 (**G**, **J**) expression in kidney tissues after Len treatment. (**K**-**N**) mRNA expression levels of CCR2 (**K**), CCR5 (**L**), CCR7 (**M**) and IL7R (**N**) were detected using qRT-PCR. Data are presented as means ± SEM, $n = 5$; *$P < 0.05$, **$P < 0.01$, ***$P < 0.001$. Scale bar = 50 μm

and cell damage in a mouse model of diabetic nephropathy [43]. Notably, CD103$^+$DCs exacerbate renal injury by activating CD8$^+$T cells in Adriamycin nephropathy and anti-GBM nephropathy; however, inhibition of CD103$^+$DCs significantly reduces the secretion of inflammatory cytokines, such as IL-6 and IL-12, thereby alleviating renal injury and the inflammatory response [39, 42, 44]. These results highlight the potential therapeutic targeting of CD103$^+$DCs for the treatment of CKD.

WGCNA was used to identify modules associated with DCs and to construct a PPI network to identify hub genes related to DCs in the current study. CCR7, CCL22, CCR2, IKZF1, MPEG1, TLR8, IL7R, and CCR5 were the top eight genes identified. KEGG pathway and GO enrichment analyses showed that these hub genes are closely related to the chemotaxis signaling pathway and T cell differentiation. Indeed, previous studies have suggested that the expression of CCR by DCs and chemotactic responses of DCs are involved in DCs migration and intrarenal accumulation, consistent with the results of the current study [45]. Interstitial DCs, including CD103$^+$DCs, facilitate the infiltration of CD8$^+$T cells and helper T cells, and antigen presentation by DCs plays a pivotal role in T cell activation [46]. Furthermore, DEGs within the high- and low-DCs abundance subgroups were screened using three machine-learning algorithms to identify IKZF1and MPEG1as hub genes. The regulation of both MPEG1 and IKZF1 by miR-33a-3p and miR-548p has been identified, highlighting the pivotal role of these microRNAs in controlling gene expression control and disease progression. Knowing that miRNA plays a role in gene expression regulation and disease progression, the study of miRNA gene regulation network may help gain new insights to diseases diagnosis and treatment. Exploring the intricate-mediated gene regulation is important holds great for advancing our understanding of diseases diagnosis and treatment.

IKZF1/IKAROS, a crucial transcription factor in leukocyte development and may play a role in the functional activation of DCs and pro-inflammatory macrophages [47, 48]. Kadono et al. identified the Ikaros–SIRT1 signaling pathway as a regulator of the canonical macrophage inflammasome-pyroptosis pathway, resulting in distinct signatures of sterile inflammation in mouse and human ischemia-reperfusion-stressed livers. Additionally, silencing IKZF1 impairs bone marrow microenvironment commitment towards the pro-inflammatory phenotype and suppresses the inflammasome-pyroptosis pathway [47]. Previous studies identified an unrecognized element in the regulation of antigen presentation that should be considered in the signaling cascade involved in the activation of DCs [49]. Immunofluorescence staining revealed a high proportion of IKZF1$^+$CD103$^+$DCs in the renal interstitium of the IgAN mouse model. Iberdomide (CC-220) is a high-affinity cereblon ligand that facilitates ubiquitination and subsequent proteasomal degradation of Aiolos and Ikaros. In patients with systemic lupus erythematosus treated with iberdomide, a dose-dependent reduction in CD20$^+$ B cells, memory B cells undergoing conversion, and plasmacytoid dendritic cells has been reported, with an inclination towards the amelioration of systemic lupus erythematous skin manifestations associated with pDCs depletion [50]. Consistent with previous studies, we found that lenalidomide treatment in anti-Thy-1 nephritis effectively alleviates mesangial damage and matrix expansion, while also reducing the infiltration of dendritic cells, T cells, and macrophages. These findings suggest that targeting IKZF1 degradation may be a promising therapeutic strategy to mitigate renal injury and inflammatory cell infiltration, making it a potential drug for the treatment of acute inflammatory phases in IgA nephropathy.

This study has several inherent limitations. First, while bioinformatics and public datasets provide valuable insights, they also introduce selection biases due to specific inclusion criteria, potentially underrepresenting broader patient populations. Missing or incomplete clinical data may compromise the accuracy and generalizability of findings. Bioinformatics analyses often lack sufficient clinical context and fail to capture complex biological interactions in real-world scenarios. Therefore, results derived from such datasets should be clinically validated for relevance and applicability. Second, this study primarily focused on DCs and their associated genes, possibly underestimating the roles of other cell types and related genes. Investigations using cellular and animal models are ongoing to address these gaps. Finally, lenalidomide has inherent limitations, including potential hematologic toxicity, which increases infection and bleeding risks. These adverse effects may necessitate dose adjustments and vigilant blood count monitoring, complicating long-term treatment and negatively impacting quality of life.

Conclusion

This study investigated the unique immune-related biomarkers and pathways in the setting of IgAN at the transcriptional level. Using various bioinformatic techniques, IKZF1 was identified as a central biomarker involved in the underlying mechanism of the disease. Additionally, pathway enrichment analysis, was used to elucidate differences in IKZF1-associated biological pathways and immune characteristics, highlighting IKZF1^{+}DCs as promising targets for interventions.

Abbreviations

IgAN	Immunoglobulin A nephropathy
DCs	Dendritic cells
WGCNA	Weighted gene co-expression network analysis
GEO	Gene Expression Omnibus
DEGs	Differentially-expressed genes
ROC	Receiver operating characteristic
RT-qPCR	Real-time quantitative PCR
PCA	Principal component analysis
GO	Gene Ontology
KEGG	Kyoto Encyclopedia of Genes and Genomes
BP	Biological process
MF	Molecular function
CC	Cellular Component
PPI	Protein-protein interaction
TSV	Tab Separated Values
LASSO	Least absolute shrinkage and selector operation
SVMs	Support vector machines
RMSE	Root mean square error
AUC	Area under the ROC curve
GSEA	Gene set enrichment analysis
IKZF1	IKAROS
MPEG1	Macrophage-expressed gene 1
FDR	False discovery rate
PAS	Periodic acid-schiff
IF	Immunofluorescence
IHC	Immunohistochemistry
FN	Fibronectin
KIM-1	Kidney injury molecule-1
CRBN	Ubiquitin E3 ligase cereblon
CCR	C-C motif chemokine receptor
BUN	Blood urea nitrogen
SCR	Serum creatinine
UACR	Urinary albumin to creatinine ratios
PCNA	Proliferating cell nuclear antigen
gd-IgA1	Galactose-deficient IgA1

Supplementary Information

The online version contains supplementary material available at https://doi.org/10.1186/s12964-025-02196-x.

Supplementary Material 1

Acknowledgements

The authors express their gratitude to the generous contributors to the GEO database for sharing their valuable data. Furthermore, we extend our appreciation to Dr. WC Cui for providing us with the necessary data analysis.

Author contributions

Conceptualized and designed the study: FP, CJS, and JYH; Performed the experiments and analyzed the data: YNZ, YLQ, SWD, YHZ, and JKX; Wrote the manuscript and prepared the figures: FP; LLW, CYZ and XMC designed the study, provided funding and supervised its execution. Each author has reviewed and endorsed the final draft of the manuscript, making significant contributions to the article.

Funding

This work was supported by the National Natural Science Foundation of China (32141005, 32200579, 82200764). Sichuan Science and Technology Program (2025ZNSFSC1602).Young Elite Scientists Sponsorship Program by CAST (2022QNRC001), China Postdoctoral Science Foundation (2022M722276), the postdoctoral fellowship program of CPSF (GZB20240415), Postdoctoral Research Fund from West China Hospital of Sichuan University (2023HXB092).

Data availability

No datasets were generated or analysed during the current study.

Declarations

Ethics approval and consent to participate

Not applicable.

Consent for publication

Not applicable.

Competing interests

The authors declare no competing interests.

Author details

[1]School of Medicine, Nankai University, Tianjin 300071, China
[2]Department of Nephrology, First Medical Center of Chinese PLA General Hospital, National Key Laboratory of Kidney Diseases, Beijing Key Laboratory of Kidney Diseases Research, National Clinical Research Center for Kidney Diseases, Beijing 100853, China
[3]Clinical Research Center, the First Affiliated Hospital of Shantou University Medical College, Shantou, Guangdong, China
[4]School of Clinical Medicine, Beijing Tsinghua Changgung Hospital, Tsinghua University, Beijing, China
[5]Kidney Research Institute, Division of Nephrology, West China Hospital, Sichuan University, Chengdu 610041, China

Received: 28 November 2024 / Accepted: 9 April 2025
Published online: 07 May 2025

References

1. Zheng Y, Lu P, Deng Y, Wen L, Wang Y, Ma X, Wang Z, Wu L, Hong Q, Duan S, Yin Z, Fu B, Cai G, Chen X, Tang F. Single-Cell transcriptomics reveal immune mechanisms of the onset and progression of IgA nephropathy. Cell Rep. 2020;33(12):108525.
2. Pattrapornpisut P, Avila-Casado C, Reich HN, Nephropathy IA. Core curriculum 2021. Am J Kidney Diseases: Official J Natl Kidney Foundation. 2021;78(3):429–41.
3. Floege J, Wied S, Rauen T. Assessing prognosis in IgA nephropathy. Kidney Int. 2022;102(1):22–4.
4. Tang R, Meng T, Lin W, Shen C, Ooi JD, Eggenhuizen PJ, Jin P, Ding X, Chen J, Tang Y, Xiao Z, Ao X, Peng W, Zhou Q, Xiao P, Zhong Y, Xiao X. A Partial Picture of the Single-Cell Transcriptomics of Human IgA Nephropathy, Frontiers in immunology 12 (2021) 645988.
5. Zeng H, Wang L, Li J, Luo S, Han Q, Su F, Wei J, Wei X, Wu J, Li B, Huang J, Tang P, Cao C, Zhou Y, Yang Q. Single-cell RNA-sequencing reveals distinct immune cell subsets and signaling pathways in IgA nephropathy. Cell Bioscience. 2021;11(1):203.
6. Esteve Cols C, Graterol Torres FA, Quirant Sánchez B, Marco H, Rusiñol MI, Navarro Díaz J, Ara Del Rey EM. Martínez Cáceres, immunological pattern in IgA nephropathy. Int J Mol Sci 21(4) (2020).
7. Pawluczyk IZA, Soares MSF, Barratt WA, Brown JR, Bhachu JS, Selvaskandan H, Zeng Y, Sarania R, Molyneux K, Roberts ISD, Barratt J. Macrophage interactions with collecting duct epithelial cells are capable of driving tubulointerstitial inflammation and fibrosis in Immunoglobulin A nephropathy, nephrology, dialysis, transplantation: official publication of the European Dialysis and transplant association -. Eur Ren Association. 2020;35(11):1865–77.
8. Myllymäki JM, Honkanen TT, Syrjänen JT, Helin HJ, Rantala IS, Pasternack AI, Mustonen JT. Severity of tubulointerstitial inflammation and prognosis in Immunoglobulin A nephropathy. Kidney Int. 2007;71(4):343–8.

9. Ertuglu LA, Kirabo A. Dendritic cell epithelial sodium channel in inflammation, Salt-Sensitive hypertension, and kidney damage. Kidney360. 2022;3(9):1620–9.
10. Zheng N, Xie K, Ye H, Dong Y, Wang B, Luo N, Fan J, Tan J, Chen W, Yu X. TLR7 in B cells promotes renal inflammation and Gd-IgA1 synthesis in IgA nephropathy. JCI Insight 5(14) (2020).
11. Nakamura Y, Inoue T. Tolerogenic dendritic cells: promising cell therapy for acute kidney injury. Kidney Int. 2023;104(3):420–2.
12. Lin CC, Chang TY, Lu YC, Wu YS, Huang W, Lo WC, Liu GF, Hsu WC, Ohashi PS, Mak TW, Fuh JL, Chen HC, Tarng DC, Chen NJ. TREM-2 mediates dendritic cell-induced NO to suppress Th17 activation and ameliorate chronic kidney diseases. J Mol Med. 2022;100(6):917–31.
13. Park S, Lee H, Lee J, Lee S, Cho S, Huh H, Kim JY, Park M, Lee S, Kim Y, Choi M, Joo KW, Kim YS, Yang SH, Kim DK. RNA-seq profiling of tubulointerstitial tissue reveals a potential therapeutic role of dual anti-phosphatase 1 in glomerulonephritis. J Cell Mol Med. 2022;26(12):3364–77.
14. Langfelder P, Horvath S. WGCNA: an R package for weighted correlation network analysis. BMC Bioinformatics. 2008;9:559.
15. Yu H, Gu L, Du L, Dong Z, Li Z, Yu M, Yin Y, Wang Y, Yu L, Ma H. Identification and analysis of key hypoxia- and immune-related genes in hypertrophic cardiomyopathy. Biol Res. 2023;56(1):45.
16. Zhang L, Zhang K, Liu S, Zhang R, Yang Y, Wang Q, Zhao S, Yang L, Zhang Y, Wang J. Identification of a CeRNA network in lung adenocarcinoma based on integration analysis of Tumor-Associated macrophage signature genes. Front Cell Dev Biology. 2021;9:629941.
17. Liu K, Chen S, Lu R. Identification of important genes related to ferroptosis and hypoxia in acute myocardial infarction based on WGCNA. Bioengineered. 2021;12(1):7950–63.
18. Yang J, Zhang J, Fan R, Zhao W, Han T, Duan K, Li X, Zeng P, Deng J, Zhang J, Yang X. Identifying potential candidate hub genes and functionally enriched pathways in the immune responses to quadrivalent inactivated influenza vaccines in the elderly through Co-Expression network analysis. Front Immunol. 2020;11:603337.
19. Guo C, Gao YY, Ju QQ, Zhang CX, Gong M, Li ZL. The landscape of gene co-expression modules correlating with prognostic genetic abnormalities in AML. J Translational Med. 2021;19(1):228.
20. Gao X, Guo Z, Wang P, Liu Z, Wang Z. Transcriptomic analysis reveals the potential crosstalk genes and immune relationship between IgA nephropathy and periodontitis. Front Immunol. 2023;14:1062590.
21. Qiu X, Quan G, Ou W, Wang P, Huang X, Li X, Shen Y, Yang W, Wang J, Wu X. Unraveling TIMP1: a multifaceted biomarker in colorectal cancer. Front Genet. 2023;14:1265137.
22. Festing MF. On determining sample size in experiments involving laboratory animals. Lab Anim. 2018;52(4):341–50.
23. Meng T, Li X, Ao X, Zhong Y, Tang R, Peng W, Yang J, Zou M, Zhou Q. Hemolytic Streptococcus May exacerbate kidney damage in IgA nephropathy through CCL20 response to the effect of Th17 cells. PLoS ONE. 2014;9(9):e108723.
24. Li Y, Xia M, Peng L, Liu H, Chen G, Wang C, Yuan D, Liu Y, Liu H. Downregulation of miR–214-3p attenuates mesangial hypercellularity by targeting PTEN–mediated JNK/c-Jun signaling in IgA nephropathy. Int J Biol Sci. 2021;17(13):3343–55.
25. Zhang M, Wu L, Deng Y, Peng F, Wang T, Zhao Y, Chen P, Liu J, Cai G, Wang L, Wu J, Chen X. Single cell dissection of Epithelial-Immune cellular interplay in acute kidney injury microenvironment. Front Immunol. 2022;13:857025.
26. He J, Peng F, Chang J, Zhao Y, Qu Y, Liu J, Liu R, Li P, Cai G, Hong Q, Chen X. The therapeutic effect of Shenhua tablet against mesangial cell proliferation and renal inflammation in mesangial proliferative glomerulonephritis. Volume 165. Biomedicine & pharmacotherapy = Biomedecine & pharmacotherapie; 2023. p. 115233.
27. Levy M, Berger J. Worldwide perspective of IgA nephropathy. Am J Kidney Diseases: Official J Natl Kidney Foundation. 1988;12(5):340–7.
28. Rajasekaran A, Green TJ, Renfrow MB, Julian BA, Novak J, Rizk DV. Current Understanding of Complement Proteins as Therapeutic Targets for the Treatment of Immunoglobulin A Nephropathy, Drugs (2023).
29. Rajasekaran A, Julian BA, Rizk DV. IgA nephropathy: an interesting autoimmune kidney disease. Am J Med Sci. 2021;361(2):176–94.
30. Selvaskandan H, Barratt J, Cheung CK. Immunological drivers of IgA nephropathy: exploring the mucosa-kidney link. Int J Immunogenet. 2022;49(1):8–21.
31. Sakai H. Cellular immunoregulatory aspects of IgA nephropathy. Am J Kidney Diseases: Official J Natl Kidney Foundation. 1988;12(5):430–2.
32. Han Z, Chen L, Peng H, Zheng H, Lin Y, Peng F, Fan Y, Xie X, Yang S, Wang Z, Yuan L, Wei X, Chen H. The role of thyroid hormone in the renal immune microenvironment. Int Immunopharmacol. 2023;119:110172.
33. Newman AM, Liu CL, Green MR, Gentles AJ, Feng W, Xu Y, Hoang CD, Diehn M, Alizadeh AA. Robust enumeration of cell subsets from tissue expression profiles. Nat Methods. 2015;12(5):453–7.
34. Du W, Gao CY, You X, Li L, Zhao ZB, Fang M, Ye Z, Si M, Lian ZX, Yu X. Increased proportion of follicular helper T cells is associated with B cell activation and disease severity in IgA nephropathy. Front Immunol. 2022;13:901465.
35. Gammon JM, Tostanoski LH, Adapa AR, Chiu YC, Jewell CM. Controlled delivery of a metabolic modulator promotes regulatory T cells and restrains autoimmunity. J Controlled Release: Official J Controlled Release Soc. 2015;210:169–78.
36. Thwe PM, Amiel E. The role of nitric oxide in metabolic regulation of dendritic cell immune function. Cancer Lett. 2018;412:236–42.
37. Rogers NM, Ferenbach DA, Isenberg JS, Thomson AW, Hughes J. Dendritic cells and macrophages in the kidney: a spectrum of good and evil, nature reviews. Nephrology. 2014;10(11):625–43.
38. Cuzic S, Ritz E, Waldherr R. Dendritic cells in glomerulonephritis, Virchows Archiv. B, Cell pathology including molecular pathology 62(6) (1992) 357–63.
39. Wang R, Chen T, Wang C, Zhang Z, Wang XM, Li Q, Lee VWS, Wang YM, Zheng G, Alexander SI, Wang Y, Harris DCH, Cao Q. Flt3 Inhibition alleviates chronic kidney disease by suppressing CD103 + dendritic cell-mediated T cell activation, nephrology, dialysis, transplantation: official publication of the European Dialysis and transplant association -. Eur Ren Association. 2019;34(11):1853–63.
40. Liu Y, Gong Y, Xu G. The role of mononuclear phagocyte system in IgA nephropathy: pathogenesis and prognosis. Front Immunol. 2023;14:1192941.
41. Wang Y, Hu Z, Wu J, Wang P, Yang Q, Li Y, Zhu F, Yang J, Deng Y, Han M, Yao Y, Zeng R, Pei G, Xu G. High renal DC-SIGN(+) cell density is associated with severe renal lesions and poor prognosis in patients with Immunoglobulin A nephropathy. Histopathology. 2019;74(5):744–58.
42. Evers BD, Engel DR, Böhner AM, Tittel AP, Krause TA, Heuser C, Garbi N, Kastenmüller W, Mack M, Tiegs G, Panzer U, Boor P, Ludwig-Portugall I, Kurts C. CD103 + Kidney dendritic cells protect against crescentic GN by maintaining IL-10-Producing regulatory T cells. J Am Soc Nephrology: JASN. 2016;27(11):3368–82.
43. Zhang F, Wang C, Wen X, Chen Y, Mao R, Cui D, Li L, Liu J, Chen Y, Cheng J, Lu Y. Mesenchymal stem cells alleviate rat diabetic nephropathy by suppressing CD103(+) DCs-mediated CD8(+) T cell responses. J Cell Mol Med. 2020;24(10):5817–31.
44. Chen T, Cao Q, Wang R, Zheng G, Azmi F, Lee VW, Wang YM, Li H, Yu D, Rogers NM, Alexander SI, Harris DCH, Wang Y. Attenuation of renal injury by depleting cDC1 and by repurposing Flt3 inhibitor in anti-GBM disease, clinical immunology (Orlando. Fla). 2023;250:109295.
45. Coates PT, Colvin BL, Ranganathan A, Duncan FJ, Lan YY, Shufesky WJ, Zahorchak AF, Morelli AE, Thomson AW. CCR and CC chemokine expression in relation to Flt3 ligand-induced renal dendritic cell mobilization. Kidney Int. 2004;66(5):1907–17.
46. Cao Q, Lu J, Li Q, Wang C, Wang XM, Lee VW, Wang C, Nguyen H, Zheng G, Zhao Y, Alexander SI, Wang Y, Harris DC. CD103 + Dendritic cells elicit CD8 + T cell responses to accelerate kidney injury in adriamycin nephropathy. J Am Soc Nephrology: JASN. 2016;27(5):1344–60.
47. Kadono K, Kageyama S, Nakamura K, Hirao H, Ito T, Kojima H, Dery KJ, Li X. Kupiec-Weglinski, myeloid Ikaros-SIRT1 signaling axis regulates hepatic inflammation and pyroptosis in ischemia-stressed mouse and human liver. J Hepatol. 2022;76(4):896–909.
48. Allman D, Dalod M, Asselin-Paturel C, Delale T, Robbins SH, Trinchieri G, Biron CA, Kastner P, Chan S. Ikaros is required for plasmacytoid dendritic cell differentiation. Blood. 2006;108(13):4025–34.
49. Movassagh M, Laderach D, Galy A. Proteins of the Ikaros family control dendritic cell maturation required to induce optimal Th1 T cell differentiation. Int Immunol. 2004;16(6):867–75.
50. Furie RA, Hough DR, Gaudy A, Ye Y, Korish S, Delev N, Weiswasser M, Zhan X, Schafer PH, Werth VP. Iberdomide in patients with systemic lupus erythematosus: a randomised, double-blind, placebo-controlled, ascending-dose, phase 2a study. Lupus Sci Med 9(1) (2022).

Publisher's note